Precambrian Research 380 (2022) 106812

Contents lists available at ScienceDirect

Precambrian Research

journal homepage: www.elsevier.com/locate/precamres

High atmospheric CO_2 levels in the early Mesoproterozoic estimated from paired carbon isotopic records from carbonates from North China

Tonggang Zhang [a,*], Menghan Li [b], Xiaoyan Chen [b], Tieguan Wang [a], Yanan Shen [b]

[a] College of Geosciences, China University of Petroleum, Beijing 102249, China
[b] School of Earth and Space Sciences, University of Science and Technology of China, Hefei 230026, China

ARTICLE INFO

Keywords:
Mesoproterozoic
Carbon isotopes
Atmospheric CO_2
Greenhouse environment

ABSTRACT

It is hypothesized that the Mesoproterozoic was characterized by a prevailing warm climate and a high atmospheric pCO_2 level. However, quantitative constraints on Mesoproterozoic atmospheric pCO_2 are scarce. Here, we report high-resolution organic and inorganic carbon isotope records from sediment samples aged ~1.6 Ga, collected from Hebei Province in North China. The $\delta^{13}C_{org}$ values of these Mesoproterozoic samples vary from −28.4‰ to −34.3‰, and the $\delta^{13}C_{carbonate}$ values range from −2.1‰ to 0.4‰. The paired carbonate and organic carbon isotope records can be used as a proxy to quantify the atmospheric CO_2 concentration during the Mesoproterozoic. According to the calibration between the photosynthetic isotopic effect and atmospheric CO_2, atmospheric CO_2 concentrations are estimated to be within the range of 910–18,800 ppmv, ~2–50 times greater than the present atmospheric level. The results support the previous hypothesis which suggests that high levels of atmospheric CO_2 prevailed in the Early Mesoproterozoic. High atmospheric pCO_2 levels could have played an important role in compensating for the possible lower solar luminosity and maintaining the temperature of the Mesoproterozoic Earth's surface.

1. Introduction

The Proterozoic witnessed a series of major changes in the atmosphere, hydrosphere, lithosphere and biosphere, and thus it has attracted much research interest in the context of the evolution of its environment and biota (Schopf and Klein, 1992; Hoffman et al., 1998, 2017; Butterfield, 2009; Kah and Bartley, 2011). The Paleoproterozoic experienced the Great Oxidation Event (Farquhar et al., 2000), while the Neoproterozoic is noted for the breakup of Rodinia, the "Snowball Earth Event" (Hoffman et al, 1998; 2017), and the Ediacaran Metazoan radiation (Xiao and Laflamme, 2009; Droser et al., 2017). Relative to the Paleoproterozoic and Neoproterozoic, the Mesoproterozoic (1.6–1.0 Ga) has received less research attention. The Mesoproterozoic was regarded as a long interval of relative stability in terms of tectonic activity, the carbon cycle, global climate, and surface oxidation state and thus has been described as a "boring" period (Buick et al., 1995). However, several new lines of evidence suggest that the Mesoproterozoic may not have been "boring" in terms of the climate and the biosphere (e.g., Kasting and Ono, 2006). For example, during the Mesoproterozoic, both red and green algae evolved, as well as fungi and calcifying cyanobacteria (e.g., Riding, 2000; Douzery et al., 2004), and marine stromatolites were well developed (Grotzinger, 1990; Awramik and Sprinkle, 1999). The rapid evolution of algae and the peak in stromatolite abundance were attributed to the evolution of CO_2-concentrating mechanisms by cyanobacteria (Riding, 2000). It is proposed that during the warm climate of the Mesoproterozoic the pCO_2 fell continuously (Kasting, 1993; Kasting and Ono, 2006; Sheldon, 2006, 2013; Sheldon et al., 2021). The concentration of atmospheric greenhouse gases such as CO_2 and CH_4 must have been much higher than those of today to compensate for the low solar luminosity experienced by the early Earth (Kasting, 1993). However, quantitative constraints on the Mesoproterozoic atmospheric pCO_2 remain scarce. According to paleosols data, Sheldon (2006, 2013) proposed that atmospheric pCO_2 fell from 20 times the present atmospheric level (PAL) to < 10 PAL during 1.8–1.1 Ga, and Retallack et al. (2021) also reported atmospheric pCO_2 with the range of 1031–1521 ppm during 1794–1732 Ma.

According to observations and experiments, photosynthetic carbon isotope fractionation (ε_p) has been demonstrated to be associated with the concentration of aqueous CO_2 (C_e), usually maintaining an equilibrium with atmospheric pCO_2 through air-seawater exchange (Weiss, 1974), and the relationship between ε_p and C_e can be quantified (Freeman and Hayes, 1992, Laws et al., 1995; Bidigare et al., 1997; Popp

* Corresponding author.
E-mail address: zhang.tonggang@cup.edu.cn (T. Zhang).

https://doi.org/10.1016/j.precamres.2022.106812
Received 28 February 2022; Received in revised form 27 May 2022; Accepted 26 July 2022
Available online 31 August 2022

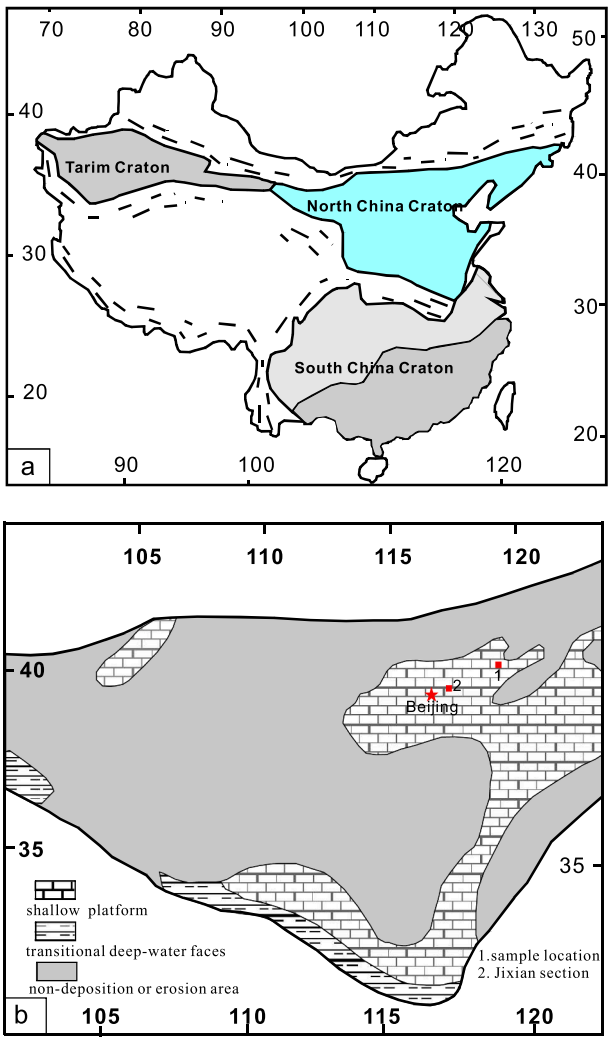

Fig. 1. Outline tectonic map of China showing the major Proterozoic blocks and Mesoproterozoic sedimentary environment of the North China Block.

et al., 1998). Thus, carbon isotopic records from sedimentary organic matter and carbonate can be used to investigate variations in atmospheric pCO_2 in the geologic past (Dean et al., 1986; Popp et al., 1989; Rau et al., 1989; Freeman and Hayes, 1992; Kump and Arthur, 1999). Primary carbon isotopic compositions may be influenced by diagenetic alternation, however, if sufficient sampling is performed for a given time interval, temporal trends in global averages could still provide a measure of changes in atmospheric pCO_2 over geological time (Kump and Arthur, 1999). Based on organic carbon isotope records from microfossils and the average of inorganic carbon isotope ratios in coeval carbonates, Kaufman and Xiao (2003) suggested that Mesoproterozoic atmospheric CO_2 concentrations were 10–200 times higher than the PAL. The analysis of both inorganic and organic carbon isotopic compositions on the same samples is essential for calculating the photosynthetic isotope effect, and to avoid the persistent problem of the correlation between carbonate and shale-dominated sequences (Kump and Arthur, 1999). In this study, we report high-resolution paired organic and inorganic carbon isotope records of sediment samples aged ~1.6 Ga from Hebei Province in North China. We use paired carbonate and organic carbon isotope records as a proxy to constrain atmospheric pCO_2 during the Mesoproterozoic.

2. Geological setting

2.1. Regional geology

Proterozoic carbonate strata are well preserved across the North China craton, where they unconformably overlie Archean and Paleoproterozoic basement lithologies (Fig. 1a). The most extensive Proterozoic sedimentary sequences occur within the Yanshan Basin in the northern part of the craton (Chen et al., 1980, Fig. 1). The Yanshan Basin represents a continental rift basin that developed at the margin of the eastern North China Block, potentially associated with the breakup of the supercontinent of Columbia at ~1.8 Ga (Lu et al., 2008; Rogers and Santosh, 2002; Zhao et al., 2004). From the Paleoproterozoic to the early Neoproterozoic, a shallow oceanic environment was developed and very thick carbonate-dominated successions were precipitated in the Yanshan Basin (Chen et al., 1980; Lu et al., 1996; Fig. 1b).

2.2. Stratigraphy

During the past several decades, the lithology, stratigraphy, biostratigraphy, and sedimentology of the Proterozoic successions of the North China Block have been extensively investigated (Chen et al., 1980; Lu et al., 1996; Zhao et al., 1997; Zhu et al., 1994, 2005). The Proterozoic sedimentary sequence in the Yanshan Basin is divided into 3 groups and 12 formations, in ascending order: (1) the Changcheng Group, composed of the Changzhougou, Chuanlinggou, Tuanshanzi, and Dahongyu formations; (2) the Jixian Group, composed of the Gaoyuzhuang, Yangzhuang, Wumishan, Hongshuizhuang, and Tieling formations; and (3) the Qingbaikou Group, consisting of the Xiamaling, Changlongshan, and Jingeryu formations (Chen et al., 1980; Lu et al., 1996). Traditionally, the Changcheng and Jixian group were regarded as Mesoproterozoic strata, and the Qingbaikou Group was regarded as Neoproterozoic strata (Chen et al., 1980). However, new geochronological data suggest that the Changcheng Group consists of Paleoproterozoic strata, the Jixian group and the Xiamaling Formation are constrained to the Mesoproterozoic, and the Jingeryu Formation to the Neoproterozoic (Lu et al, 2008).

The Gaoyuzhuang Formation is of interest here because the carbonates samples from this formation are suitable for measurements of the carbon isotope compositions of both inorganic and organic carbon in the same sample, owing to the well-preserved state of the organic matter in the carbonates. Basis on lithology, the Gaoyuzhuang Formation is subdivided into four members, in ascending order (Chen et al., 1980). The first member is divided into gray cherty, stromatolitic dolomicrite, interbedded with sandy to shaley dolomicrite. The second member is subdivided into two parts; the lower part consists of dark-gray thin-bedded muddy Mn-rich dolomicrite with dolomitic siltstone, and the upper part consists of dark-gray Mn-rich thick-bedded to massive dolostones. The third member is composed of dark-grey, black organic-rich, muddy dolomicrite with cherty concretions. The fourth member consists of grey thick-bedded to massive dolomicrite with cherty concretions.

2.3. Geochronology

A single grain zircon U–Pb age of 1625 ± 6.2 Ma from volcanic rocks in the underlying Dahongyu Formation constrains the age of the base of the Gaoyuzhuang Formation to ~1600 Ma (Lu and Li, 1991). This locates the Mesoproterozoic–Paleoproterozoic boundary to between the Gaoyuzhuang Formation and the underlying Dahongyu Formation. A zircon U–Pb age of 1560 ± 5 Ma from the upper Gaoyuzhuang Formation (Li et al., 2010) constrains the age of the Gaoyuzhuang Formation to the range of 1600–1500 Ma.

3. Analytical methods

3.1. Sample collection

For geochemical analysis, more than 400 carbonate samples from the Gaoyuzhang Formation were collected from a drill core from well JQ3, in Kuancheng County of Hebei Province, North China (Fig. 1b). The strata drilled in well JQ3 have a thickness of 500 m and are comprise the second and the third members of the Gaoyuzhang Formation. Compared to outcrop sampling, the drill-core samples avoided possible weathering effects and hence they can potentially provide more reliable carbon isotope records. The drill-core samples were cut to remove calcite dykes and were cleaned with distilled water to avoid the influence of drilling fluid. The samples were then milled into powder for geochemical analyses. 380 samples were measured for TOC and $\delta^{13}C_{org}$, and 180 samples were analyzed for $\delta^{13}C_{carb}$ and $\delta^{18}O$.

3.2. Carbonate carbon ($\delta^{13}C_{carb}$) and oxygen isotopes ($\delta^{18}O$)

The carbon and oxygen isotopic compositions of the carbonate samples were measured using the traditional acid release method: ~20 mg of powdered sample was reacted with anhydrous H_3PO_4 at 25°C for 24 h under vacuum to liberate CO_2, and the CO_2 was then purified in a high vacuum extraction line and sealed in a Pyrex break-seal tube for carbon isotope analysis. The carbon isotopic ratios were analyzed on a Finnigan MAT 253 mass spectrometer. The results are reported using the standard per mil δ notation relative to the V-PDB standard ($\delta^{13}C$ and $\delta^{18}O$). Analytical precision of the analyses is better than 0.1‰.

3.3. Total organic carbon (TOC) and organic carbon isotopes ($\delta^{13}C_{org.}$)

For organic carbon analysis, ~2 g of powdered sample was treated with 6 N HCl for 24 h to remove carbonates, and the residue was then washed and filtered. After drying and weighing the residue was used for TOC and organic carbon isotope analyses. The TOC was measured with an infrared spectrometry carbon–sulfur analyzer. Carbonate-free samples of ~100 mg were weighed and then combusted in the oven of the carbon–sulfur analyzer, and the organic carbon content was determined by infrared spectrometry based on the CO_2 produced during combustion. The analytical reproducibility was ~0.1%.

Organic carbon isotope compositions were analyzed online using an auto-sampler Flash EA 2000 interfaced with the MAT 253 IR-MS. Based on the predetermined organic carbon concentration, samples of 100 μg to 10 mg were weighed and combusted in the elemental analyzer, and the pure CO_2 gas was introduced into the mass spectrometer for $^{13}C/^{12}C$ determination. The organic carbon isotope results are reported using the standard per mil δ notation relative to the V-PDB standard ($\delta^{13}C$). Analytical precision was ~0.2‰.

Finally, phosphorus (P_2O_5) concentrations in the sedimentary rocks of the Gaoyuzhuang Formation were measured by X-ray fluorescence spectrometer (XRF). Around 0.7 g of powdered sample was mixed with $Li_2B_4O_7$, the mixture was then combusted in a platinum crucible at 1200℃ for 15 min, and then pressed into 30-mm diameter discs in a platinum mold at 800℃. The discs sample was measured by XRF to determine the element content. The analytical reproducibility was ~0.01%.

4. Results and discussion

4.1. Evaluation of diagenetic alternation

Several factors could potentially alter the primary carbon isotopic composition of organic matter within the Mesoproterozoic samples. The first is the origin of the organic matter contributing to the C isotopic composition. Retallack et al. (2021) provided evidence of microbial life on land during the Paleoproterozoic, and therefore terrestrial organic carbon input into the ocean may influence the $\delta^{13}C_{org}$ values. However, the influence of terrestrial organic carbon input on the $\delta^{13}C_{org}$ values may be minor due to the insignificant terrigenous input for carbonate deposits and the absence of land plants during the Mesoproterozoic (e.g.,

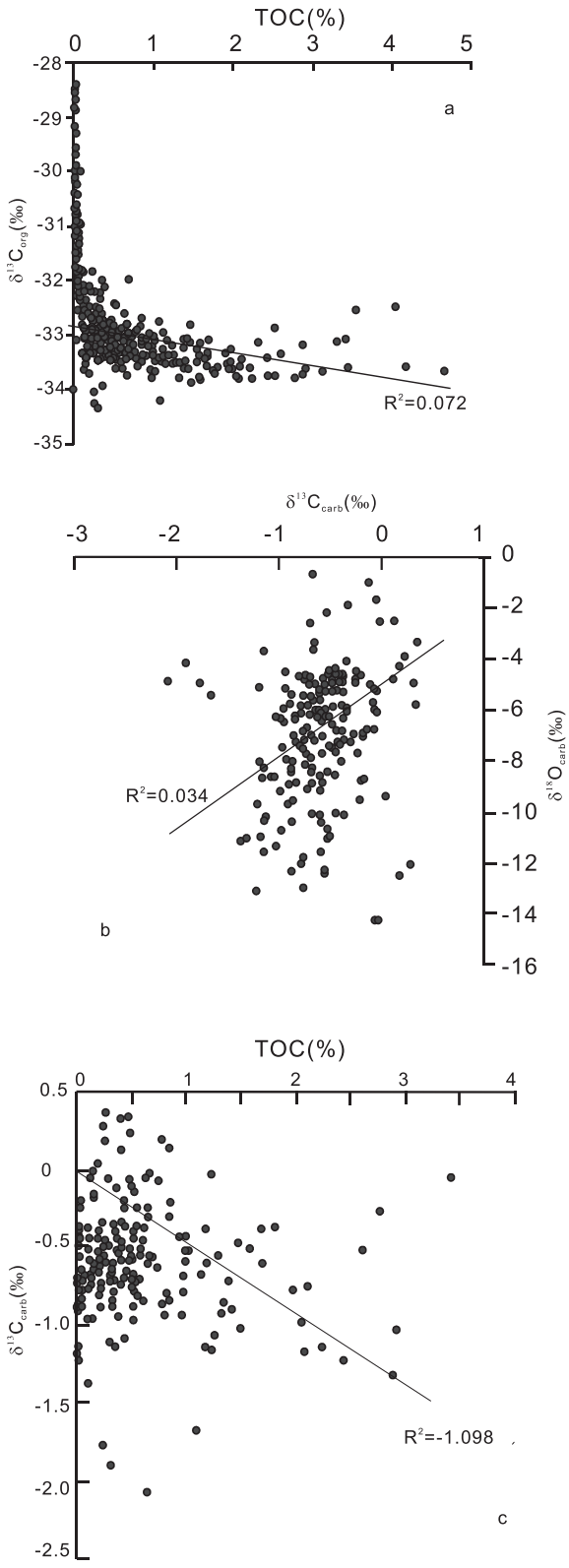

Fig. 2. Evaluation of diagenetic influences on primary carbon isotope records. (a) Crossplot of $\delta^{13}C_{org}$ and TOC. (b) Crossplot of $\delta^{13}C_{carb}$ and $\delta^{18}O_{carb.}$ (c) Crossplot of $\delta^{13}C_{carb}$ and TOC.

Table 1
$\delta^{13}C_{org}$, $\delta^{13}C_{carb}$, $\delta^{18}O_{carb}$ values, TOC and P content for the Mesoproterozoic samples from well JQ3 of the Gaoyuzhang Formation in North China.

Well	depth (m)	lithology	TOC (%)	$\delta^{13}C_{org}$ (‰)	$\delta^{13}C_{carb}$ (‰)	$\delta^{18}O_{carb}$ (‰)	P (%)
JQ3	8.6	carbonate	0.22	–32.9	−0.6	−5.4	
JQ3	10.5	carbonate	0.49	–33.2	−0.1	−6.8	
JQ3	11.8	carbonate	0.53	–32.4	−0.4	−8.0	
JQ3	13.6	carbonate	0.19	–32.6	0.0	−9.4	
JQ3	14.3	carbonate	0.86	–33.5	−0.3	−1.9	0.04
JQ3	17.1	carbonate	0.53	–32.9	−0.4	−7.2	
JQ3	18.5	carbonate	0.52	–33.0	−0.7	−10.1	
JQ3	18.7	carbonate	0.65	–33.3	−0.3	−7.2	
JQ3	21	carbonate	0.22	–33.1	−0.7	−8.2	
JQ3	22.3	carbonate	0.23	–33.2	−0.9	−5.4	
JQ3	26.9	carbonate	0.32	–33.0	−0.8	−7.2	
JQ3	27.6	carbonate	0.11	–32.7	−0.8	−7.5	
JQ3	28.3	carbonate	0.31	–33.0	−0.7	−7.8	
JQ3	28.74	carbonate	0.21	–32.9	−0.8	−5.9	
JQ3	31	carbonate	0.97	–33.6	−0.9	−4.5	
JQ3	31.7	carbonate	0.34	–32.2	−0.8	−7.4	
JQ3	33	carbonate	0.52	–32.8	−0.7	−7.0	
JQ3	34.1	carbonate	0.56	–33.4	−0.8	−6.2	
JQ3	34.8	carbonate	0.79	–33.3	−0.9	−8.1	
JQ3	35.9	carbonate	0.65	–33.5	−0.3	−4.8	
JQ3	37	carbonate	0.61	–33.5			
JQ3	37.35	carbonate	0.21	–32.9	−0.7	−3.6	0.01
JQ3	39.5	carbonate	0.27	–33.0			
JQ3	41	carbonate	0.81	–33.6			
JQ3	42.5	carbonate	0.33	–33.2	−0.7	−0.7	
JQ3	43.6	carbonate	0.51	–33.3	−0.8	−4.7	
JQ3	43.9	carbonate	0.43	–33.0	−0.5	−4.5	
JQ3	46.3	carbonate	0.49	–33.2	−0.5	−5.2	
JQ3	46.9	carbonate	0.33	–32.8	−0.6	−5.6	
JQ3	48.3	carbonate	0.14	–32.6	−0.7	−7.0	
JQ3	48.7	carbonate	0.60	–33.1	−0.5	−8.5	
JQ3	51	carbonate	0.34	–33.3	−0.4	−5.9	
JQ3	51.7	carbonate	0.50	–33.3	−0.1	−5.0	
JQ3	53.8	carbonate	0.26	–33.0	−0.5	−4.8	
JQ3	55.6	carbonate	1.14	–33.4	−0.7	−5.6	
JQ3	57.1	carbonate	1.17	–33.4	−1.1	−3.7	
JQ3	58.3	carbonate	0.10	–32.2	−1.0	−5.9	
JQ3	59.2	carbonate	1.39	–33.6	−0.7	−5.6	
JQ3	60.5	carbonate	0.48	–33.3			
JQ3	61.1	carbonate	0.67	–33.4	−0.6	−6.4	
JQ3	62.5	carbonate	0.59	–33.4	−0.5	−6.0	
JQ3	63.3	carbonate	0.44	–33.1	−0.4	−6.3	
JQ3	65.3	carbonate	0.37	–33.1	−0.5	−2.2	
JQ3	66.7	carbonate	0.59	–33.6	−0.7	−5.0	0.03
JQ3	67.5	carbonate	0.46	–33.2	−0.7	−3.4	
JQ3	69	carbonate	0.23	–32.8	−0.8	−5.4	
JQ3	71.1	carbonate	1.81	–33.6	−0.4	−4.6	
JQ3	72	carbonate	0.89	–33.4			
JQ3	73.26	carbonate	2.88	–33.2			
JQ3	74.1	carbonate	0.41	–33.3	−0.3	−4.1	
JQ3	76	carbonate	0.31	–33.3			
JQ3	76.9	carbonate	0.21	–33.1	−0.4	−4.9	
JQ3	77.7	carbonate	0.80	–33.6	−0.9	−5.2	
JQ3	78.8	carbonate	0.38	–33.3	−0.5	−4.6	
JQ3	80	carbonate	1.26	–33.4	−1.1	−8.6	
JQ3	80.9	carbonate	1.39	–33.2			
JQ3	81.66	carbonate	0.87	–33.3			
JQ3	82	carbonate	0.74	–33.2			
JQ3	83.8	carbonate	0.33	–33.1	−0.6	−5.0	
JQ3	84.75	carbonate	0.85	–33.4			
JQ3	85.75	carbonate	0.68	–33.3			
JQ3	86.7	carbonate	0.27	–33.3			
JQ3	87.4	carbonate	0.27	–32.7	−0.5	−4.9	
JQ3	89.7	carbonate	1.19	–33.4	−0.6	−6.0	0.05
JQ3	90.3	carbonate	0.34	–32.6			
JQ3	92.4	carbonate	0.62	–33.2	−0.4	−4.9	
JQ3	94	carbonate	0.34	–32.9	−0.7	−4.7	
JQ3	95.7	carbonate	0.37	–32.9	−0.1	−1.0	
JQ3	96.5	carbonate	0.24	–33.2	−0.6	−4.8	
JQ3	97.6	carbonate	0.74	–33.3	−0.6	−6.2	
JQ3	99.3	carbonate	0.23	–32.9	−0.6	−7.7	
JQ3	100.8	carbonate	0.41	–33.2	0.1	−4.8	
JQ3	102.6	carbonate	0.35	–32.7	−0.4	−6.7	
JQ3	104	carbonate	0.49	–32.9	0.2	−3.9	

(*continued on next page*)

Table 1 (*continued*)

Well	depth (m)	lithology	TOC (%)	$\delta^{13}C_{org}$ (‰)	$\delta^{13}C_{carb}$ (‰)	$\delta^{18}O_{carb}$ (‰)	P (%)
JQ3	105	carbonate	0.40	–33.0	−0.5	−5.9	
JQ3	105.8	carbonate	1.68	–33.3	−0.4	−5.8	
JQ3	107.9	carbonate	0.94	–33.0	−0.4	−7.3	
JQ3	108.7	carbonate	0.65	–33.0	−0.6	−8.6	
JQ3	109.4	carbonate	0.41	–32.7	−0.7	−7.2	
JQ3	110.3	carbonate	0.97	–33.2	−0.7	−5.4	
JQ3	111.4	carbonate	1.07	–32.8			
JQ3	112.3	carbonate	1.17	–33.1	−0.4	−7.2	
JQ3	113.4	carbonate	0.78	–32.9			
JQ3	113.7	carbonate	3.42	–33.1	0.0	−5.2	
JQ3	115.1	carbonate	0.41	–32.8	−0.6	−8.8	0.02
JQ3	116.6	carbonate	1.69	–33.1	−0.6	−10.1	
JQ3	117.6	carbonate	0.98	–33.8	−0.8	−12.0	
JQ3	118.4	carbonate	2.78	–33.8	−0.3	−7.0	
JQ3	118.7	carbonate	0.64	–32.6	−0.1	−14.2	
JQ3	120.7	carbonate	0.44	–32.8	−0.2	−8.8	
JQ3	121.4	carbonate	0.15	–32.2			
JQ3	123.5	carbonate	0.55	–33.1	−0.4	−7.2	
JQ3	123.75	carbonate	0.48	–33.0			
JQ3	125.4	carbonate	0.67	–33.1	0.0	−6.1	
JQ3	127.6	carbonate	1.23	–33.2	0.0	−14.3	
JQ3	128.9	carbonate	1.59	–33.2	−0.5	−11.0	
JQ3	129.1	carbonate	0.59	–32.9	−0.5	−7.4	
JQ3	130.5	carbonate	0.44	–33.1	−0.3	−4.9	
JQ3	132	carbonate	0.40	–32.9	0.3	−4.9	
JQ3	134	carbonate	0.84	–33.2			
JQ3	137.4	carbonate	0.25	–32.7	−0.6	−6.2	
JQ3	138.4	carbonate	1.40	–33.2			
JQ3	139.8	carbonate	1.03	–33.1			
JQ3	140.2	carbonate	0.56	–33.1	−0.2	−4.5	
JQ3	142.7	carbonate	0.30	–32.6	−0.5	−5.1	0.01
JQ3	143.9	carbonate	1.00	–33.0			
JQ3	146	carbonate	0.50	–32.8			
JQ3	146.4	carbonate	0.78	–32.9	0.2	−4.3	
JQ3	147.6	carbonate	0.28	–32.7	0.4	−3.3	
JQ3	148.5	carbonate	0.47	–32.7	0.3	−5.8	
JQ3	149	carbonate	0.29	–32.6	−0.1	−6.0	
JQ3	149.4	carbonate	0.51	–33.0			
JQ3	150.3	carbonate	1.12	–33.0			
JQ3	151.6	carbonate	0.39	–32.9			
JQ3	151.8	carbonate	0.49	–33.1			
JQ3	153.1	carbonate	0.97	–33.0			
JQ3	154.3	carbonate	0.17	–32.5	−0.2	−8.7	
JQ3	154.6	carbonate	0.30	–33.1			
JQ3	156.6	carbonate	0.29	–33.1			
JQ3	157.6	carbonate	0.24	–32.9			
JQ3	161.1	carbonate	0.13	–32.4	0.0	−1.7	
JQ3	162.1	carbonate	0.31	–32.5			
JQ3	165.7	carbonate	0.15	–32.4			
JQ3	167.4	carbonate	0.17	–32.2	0.0	−2.5	
JQ3	168.3	carbonate	0.26	–32.8			
JQ3	169.6	carbonate	4.04	–32.5			
JQ3	171	carbonate	0.44	–32.9	−0.7	−8.4	
JQ3	172.1	carbonate	0.85	–32.7			
JQ3	173	carbonate	0.44	–32.8			
JQ3	173.75	carbonate	0.50	–32.9			
JQ3	175.6	carbonate	0.14	–32.2	−0.7	−7.9	0.01
JQ3	176.5	carbonate	0.53	–33.6	−0.9	−8.4	
JQ3	178.2	carbonate	0.33	–33.0	−0.9	−5.7	
JQ3	179.7	carbonate	0.26	–33.0			
JQ3	182	carbonate	0.86	–33.5	0.1	−2.5	
JQ3	182.6	carbonate	0.44	–33.4			
JQ3	183.4	carbonate	0.32	–33.3			
JQ3	184.9	carbonate	0.26	–33.1			
JQ3	185.3	carbonate	0.15	–33.3			
JQ3	188	carbonate	0.41	–33.4			
JQ3	188.6	carbonate	0.69	–33.4	−0.6	−12.4	
JQ3	191	carbonate	0.28	–33.1			
JQ3	192	carbonate	0.13	–32.5	−0.6	−10.4	
JQ3	193.5	carbonate	0.17	–33.2			
JQ3	195.1	carbonate	0.14	–33.5			
JQ3	196.69	carbonate	0.15	–33.5			
JQ3	196.8	carbonate	0.13	–33.7			
JQ3	197.85	carbonate	0.15	–33.6			
JQ3	199.7	carbonate	0.00	−34.0	−1.2	−5.1	0.02
JQ3	200.3	carbonate	0.37	–33.9			

(*continued on next page*)

Table 1 (*continued*)

Well	depth (m)	lithology	TOC (%)	$\delta^{13}C_{org}$ (‰)	$\delta^{13}C_{carb}$ (‰)	$\delta^{18}O_{carb}$ (‰)	P (%)
JQ3	202.7	carbonate	0.25	−34.0	−1.8	−4.9	
JQ3	203.6	carbonate	0.20	–33.7			
JQ3	205.2	carbonate	0.30	−34.3	−1.9	−4.1	
JQ3	206.5	carbonate	0.26	−34.3			
JQ3	207.3	carbonate	0.64	–33.1	−2.1	−4.9	
JQ3	209.5	carbonate	1.09	−34.2	−1.7	−5.4	0.08
JQ3	211.3	carbonate	0.67	–33.7			
JQ3	212.8	carbonate	1.06	–33.4			
JQ3	213.9	carbonate	1.92	–33.3			
JQ3	214.5	carbonate	2.52	–32.9			
JQ3	215.3	carbonate	0.84	–32.8	−0.8	−4.7	
JQ3	218	carbonate	0.32	–32.5	−0.7	−8.9	
JQ3	219.1	carbonate	3.30	–33.1			
JQ3	220.2	carbonate	1.97	–33.3	−0.8	−6.8	0.2
JQ3	222.3	carbonate	1.39	–33.2			
JQ3	223	carbonate	0.25	–32.6			
JQ3	224.5	carbonate	0.96	–33.1	0.3	−12.1	
JQ3	226.2	carbonate	0.87	–33.2			
JQ3	226.8	carbonate	0.85	–33.2			
JQ3	228.7	carbonate	2.61	–33.4	−0.5	−11.0	
JQ3	229.54	carbonate	0.75	–33.3			
JQ3	234.45	carbonate	1.03	–33.4	−0.6	−12.3	
JQ3	234.5	carbonate	1.29	–33.5			
JQ3	236.8	carbonate	1.41	–33.5			
JQ3	237.6	carbonate	0.26	–32.7	0.2	−12.5	0.03
JQ3	239.5	carbonate	2.43	–33.4	−1.2	−13.1	
JQ3	243.8	carbonate	1.46	–32.8	−0.5	−6.6	
JQ3	245.1	carbonate	3.45	–33.6			
JQ3	246.5	carbonate	1.58	–33.8			
JQ3	247.3	carbonate	1.32	–33.8	−0.9	−8.0	
JQ3	248.3	carbonate	0.53	–33.4	−1.0	−10.7	
JQ3	248.5	carbonate	2.53	–33.8			
JQ3	250.3	carbonate	2.07	–33.8			
JQ3	252.2	carbonate	1.48	–33.9	−1.0	−6.3	0.09
JQ3	253.9	carbonate	1.59	–33.8			
JQ3	254.8	carbonate	1.92	–33.5			
JQ3	256.7	carbonate	0.52	–32.4	−0.1	−6.8	
JQ3	258.4	carbonate	1.23	–33.5	−1.2	−8.7	
JQ3	259.5	carbonate	1.58	–33.4			
JQ3	260.7	carbonate	0.85	–33.1	−0.8	−7.3	
JQ3	261.3	carbonate	0.95	–33.2			
JQ3	262	carbonate	0.91	–33.4			
JQ3	264	carbonate	1.75	–33.6			
JQ3	265	carbonate	1.95	–33.6			
JQ3	267.6	carbonate	2.88	–33.7	−1.3	−11.1	0.17
JQ3	267.9	carbonate	4.65	–33.7			
JQ3	269.7	carbonate	2.21	–33.6			
JQ3	269.95	carbonate	0.75	–33.4			
JQ3	271	carbonate	0.99	–33.3			
JQ3	273.6	carbonate	2.00	–33.6			
JQ3	275.1	carbonate	0.55	–33.3			
JQ3	277.4	carbonate	1.00	–33.1	−0.6	−11.6	
JQ3	278.8	carbonate	2.06	–33.8	−1.0	−9.2	
JQ3	279.2	carbonate	1.02	–33.7			
JQ3	280.8	carbonate	3.13	–33.7			
JQ3	281	carbonate	0.16	–32.6	−0.2	−7.0	0.01
JQ3	283	carbonate	2.08	–33.6	−1.2	−11.0	
JQ3	283.75	carbonate	1.55	–33.5			
JQ3	285.5	carbonate	0.25	–33.0			
JQ3	286.1	carbonate	0.49	–33.0			
JQ3	286.8	carbonate	4.18	–33.6			
JQ3	288	carbonate	0.85	–33.4			
JQ3	289.3	carbonate	0.20	–32.5	−0.5	−10.7	0.01
JQ3	290.2	carbonate	1.41	–33.6	−0.9	−9.7	
JQ3	290.4	carbonate	1.15	–33.5			
JQ3	292.8	carbonate	0.77	–33.4			
JQ3	294.7	carbonate	1.64	–33.4			
JQ3	295.4	carbonate	1.97	–33.5			
JQ3	296	carbonate	0.67	–33.0			
JQ3	297.44	carbonate	0.13	–32.4	−0.7	−8.3	0.01
JQ3	297.9	carbonate	0.65	–33.3			
JQ3	299.4	carbonate	0.91	–33.0			
JQ3	299.9	carbonate	2.45	–33.8			
JQ3	300.3	carbonate	0.51	–32.9			
JQ3	301.8	carbonate	1.09	–33.5			
JQ3	302.6	carbonate	0.53	–33.1	−1.1	−11.6	0.02

(*continued on next page*)

Table 1 (*continued*)

Well	depth (m)	lithology	TOC (%)	$\delta^{13}C_{org}$ (‰)	$\delta^{13}C_{carb}$ (‰)	$\delta^{18}O_{carb}$ (‰)	P (%)
JQ3	303.6	carbonate	1.39	–33.1			
JQ3	304.9	carbonate	0.18	–32.6			
JQ3	306.2	carbonate	0.24	−31.8			
JQ3	307	carbonate	0.08	–32.3	−0.3	−6.1	
JQ3	308.1	carbonate	0.44	–33.2			
JQ3	309.7	carbonate	0.61	–33.2	−1.1	−8.6	
JQ3	310.85	carbonate	0.03	−31.1			
JQ3	312.8	carbonate	2.92	–33.6	−0.9	−8.9	
JQ3	313.5	carbonate	0.11	−31.8	−1.0	−11.4	
JQ3	315.4	carbonate	0.53	–33.2			
JQ3	316.8	carbonate	0.04	−31.5			
JQ3	317.6	carbonate	0.05	−31.4			
JQ3	318.5	carbonate	0.33	–32.8	−0.8	−8.8	0.01
JQ3	319.3	carbonate	0.86	–33.1			
JQ3	321	carbonate	0.06	−31.9	−0.2	−9.5	
JQ3	321.7	carbonate	0.28	–32.5			
JQ3	322.5	carbonate	0.20	–32.1			
JQ3	323.1	carbonate	0.27	–32.2	−0.4	−10.0	
JQ3	324.6	carbonate	0.49	–32.9			
JQ3	326.5	carbonate	0.99	–33.4			
JQ3	327.4	carbonate	3.54	–32.5	−0.4	−10.0	
JQ3	328.6	carbonate	0.06	−31.5			
JQ3	329.2	carbonate	0.14	–32.1	−0.9	−10.4	
JQ3	330.1	carbonate	0.81	–33.5			
JQ3	331.1	carbonate	0.65	–33.3			
JQ3	332.7	carbonate	0.63	–33.6			
JQ3	334.3	carbonate	0.03	−31.5	−0.8	−6.3	
JQ3	335.6	carbonate	0.06	–32.1	−0.8	−11.8	
JQ3	337.5	carbonate	2.11	–33.5			
JQ3	339	carbonate	0.29	–32.9	−0.8	−13.0	0.16
JQ3	339.7	carbonate	1.12	–33.3			
JQ3	340.4	carbonate	0.41	–33.1			
JQ3	341.6	carbonate	0.36	–33.1			
JQ3	343.5	carbonate	0.53	–33.4			
JQ3	343.9	carbonate	0.75	–33.1			
JQ3	345.6	carbonate	1.01	–33.5	−0.1	−5.7	
JQ3	349.6	carbonate	0.36	–32.6	−0.5	−8.4	
JQ3	350.2	carbonate	0.25	–32.8			
JQ3	351	carbonate	0.99	–33.4			
JQ3	352.5	carbonate	0.07	–32.2	−0.5	−6.2	
JQ3	353.1	carbonate	0.21	–32.2			
JQ3	354.9	carbonate	1.38	–33.1			
JQ3	356	carbonate	0.76	–33.0			
JQ3	356.85	carbonate	0.14	–32.2			
JQ3	358.3	carbonate	2.32	–33.1	−1.0	−7.5	
JQ3	359.7	carbonate	1.46	–33.1			
JQ3	360	carbonate	0.33	–32.3			
JQ3	362.4	carbonate	1.43	–33.1			
JQ3	362.9	carbonate	0.09	–32.4			
JQ3	364.3	carbonate	0.79	–33.4			
JQ3	366.4	carbonate	0.05	−31.4	−0.9	−9.6	
JQ3	368	carbonate	0.14	–32.5	−0.7	−7.8	
JQ3	369.9	carbonate	0.69	–33.4			
JQ3	372	carbonate	0.52	–33.5			
JQ3	372.8	carbonate	1.55	–33.3	−0.6	−8.9	
JQ3	373.8	carbonate	0.27	–32.8			
JQ3	375.3	carbonate	0.12	–32.6			
JQ3	375.45	carbonate	0.40	–33.3	−1.4	−11.2	
JQ3	376.9	carbonate	0.15	–32.6			
JQ3	378.4	carbonate	0.69	–32.0			
JQ3	379.1	carbonate	0.23	–32.9			
JQ4	381.4	carbonate	0.30	–33.5			
JQ3	381.8	carbonate	1.66	–33.6			
JQ3	384.4	carbonate	2.24	–33.8			
JQ3	384.5	carbonate	1.25	–33.5	−1.1	−10.4	
JQ3	385.4	carbonate	1.43	–33.6			
JQ3	387	carbonate	1.77	–33.7			
JQ3	388	carbonate	1.68	–33.4			
JQ3	389	carbonate	1.10	–33.5			
JQ3	390.2	carbonate	1.04	–33.5			
JQ3	390.55	carbonate	0.55	–33.2			
JQ3	391.6	carbonate	0.67	–33.2			
JQ3	392.6	carbonate	0.08	–32.6			
JQ3	393.7	carbonate	0.39	–32.1			
JQ3	393.76	carbonate	1.34	–33.5	−1.0	−6.5	
JQ3	395.4	carbonate	0.46	–33.4	−0.9	−6.2	

(*continued on next page*)

Table 1 (*continued*)

Well	depth (m)	lithology	TOC (%)	$\delta^{13}C_{org}$ (‰)	$\delta^{13}C_{carb}$ (‰)	$\delta^{18}O_{carb}$ (‰)	P (%)
JQ3	396.5	carbonate	0.12	–32.1			
JQ3	397.8	carbonate	0.30	–32.6	−0.4	−7.6	
JQ3	399.9	carbonate	0.02	−30.0			
JQ3	401.2	carbonate	0.08	−30.0	−1.2	−8.1	
JQ3	403	carbonate	0.13	–33.1			
JQ3	404.2	carbonate	0.01	−28.6			
JQ3	405.5	carbonate	0.31	–33.1	−1.2	−9.7	
JQ3	406	carbonate	0.03	−31.4	−1.1	−10.2	
JQ3	407.4	carbonate	0.02	–33.1			
JQ3	408.3	carbonate	0.05	−31.0			
JQ3	408.6	carbonate	0.02	−27.9			
JQ3	410.5	carbonate	0.03	−29.3			
JQ3	410.8	carbonate	0.03	−30.0			
JQ3	412.6	carbonate	0.01	−30.2			
JQ3	414.9	carbonate	0.01	−29.2	−0.9	−8.3	
JQ3	415.9	carbonate	0.03	−30.2			
JQ3	417.4	carbonate	0.02	−29.6			
JQ3	419.1	carbonate	0.15	–32.4	−0.9	−7.0	
JQ3	419.4	carbonate	0.03	−31.4	−0.7	−6.7	
JQ3	422.2	carbonate	0.02	−29.7			
JQ3	422.7	carbonate	0.05	−31.5	−1.1	−8.3	0.05
JQ3	423.5	carbonate	0.02	−30.4	−0.7	−7.2	
JQ3	424.9	carbonate	0.24	–32.7			
JQ3	425.4	carbonate	0.23	–33.0			
JQ3	426.4	carbonate	0.02	−30.1	−0.6	−9.2	
JQ3	427.5	carbonate	0.05	−31.4	−0.9	−8.9	
JQ3	428.8	carbonate	0.10	−31.8			
JQ3	430.8	carbonate	0.03	−29.6	−0.4	−10.1	
JQ3	431.4	carbonate	0.02	−30.8	−0.9	−12.3	
JQ3	432.7	carbonate	0.05	−30.4			
JQ3	434.4	carbonate	0.05	–32.5			
JQ3	435.5	carbonate	0.41	–33.1			
JQ3	438	carbonate	0.38	–33.2			
JQ3	439.4	carbonate	0.07	−31.2	−0.4	−5.2	
JQ3	442.7	carbonate	0.07	−31.3			
JQ3	443.2	carbonate	0.04	−30.8			
JQ3	445.8	carbonate	0.05	−30.0			0.01
JQ3	447.3	carbonate	0.04	−31.1	−0.8	−7.5	
JQ3	448.7	carbonate	0.02	−30.2	−0.7	−9.1	
JQ3	449.1	carbonate	0.03	−28.4			
JQ3	451.7	carbonate	0.18	–32.6	−0.4	−5.3	
JQ3	451.9	carbonate	0.08	−31.0	−0.6	−9.0	
JQ3	453	carbonate	0.11	–32.6			
JQ3	456.1	carbonate	0.02	−28.7			
JQ3	457.68	carbonate	0.02	−30.0	−0.7	−5.8	
JQ3	458.5	carbonate	0.05	−31.2			
JQ3	460.6	carbonate	0.04	–32.3			
JQ3	461.3	carbonate	0.03	−31.6	−0.7	−6.1	
JQ3	463	carbonate	0.06	−31.8			
JQ3	465.1	carbonate	0.05	−31.1			
JQ3	466.7	carbonate	0.03	−31.2			
JQ3	468	carbonate	0.02	−30.8			
JQ3	470	carbonate	0.02	−31.2	−0.7	−2.6	0.01
JQ3	470.9	carbonate	0.03	−31.8	−0.4	−6.8	
JQ3	472.4	carbonate	0.03	−30.9			
JQ3	473	carbonate	0.04	−31.4			
JQ3	475.2	carbonate	0.47	–32.8			
JQ3	476.7	carbonate	0.04	−31.9	−0.6	−7.0	
JQ3	477.8	carbonate	0.31	–32.7			
JQ3	478.6	carbonate	0.20	–32.7			
JQ3	479.4	carbonate	0.04	−31.2			
JQ3	480.5	carbonate	0.05	–32.0	−0.2	−4.6	
JQ3	481.6	carbonate	0.02	−31.0			
JQ3	482.5	carbonate	0.03	−29.9			
JQ3	484	carbonate	0.02	−28.5			
JQ3	486	carbonate	0.02	−28.9	−0.5	−4.6	0.01
JQ3	487.5	carbonate	0.02	−30.7			
JQ3	488.7	carbonate	0.01	−28.5	−0.4	−4.7	
JQ3	489.1	carbonate	0.01	−28.8	0.5	−2.4	
JQ3	490.15	carbonate	0.11	–32.8	−0.5	−5.2	
JQ3	491.2	carbonate	0.03	−30.0	−0.4	−4.3	0.01
JQ3	491.3	carbonate	0.03	−31.2	−0.6	−5.0	
JQ3	493.3	carbonate	0.03	−30.7			
JQ3	494.4	carbonate	0.03	−30.7			
JQ3	497.9	carbonate	0.04	−30.6	−0.2	−7.7	
JQ3	498.9	carbonate	0.02	−29.6			
JQ3	500	carbonate	0.03	−30.2			

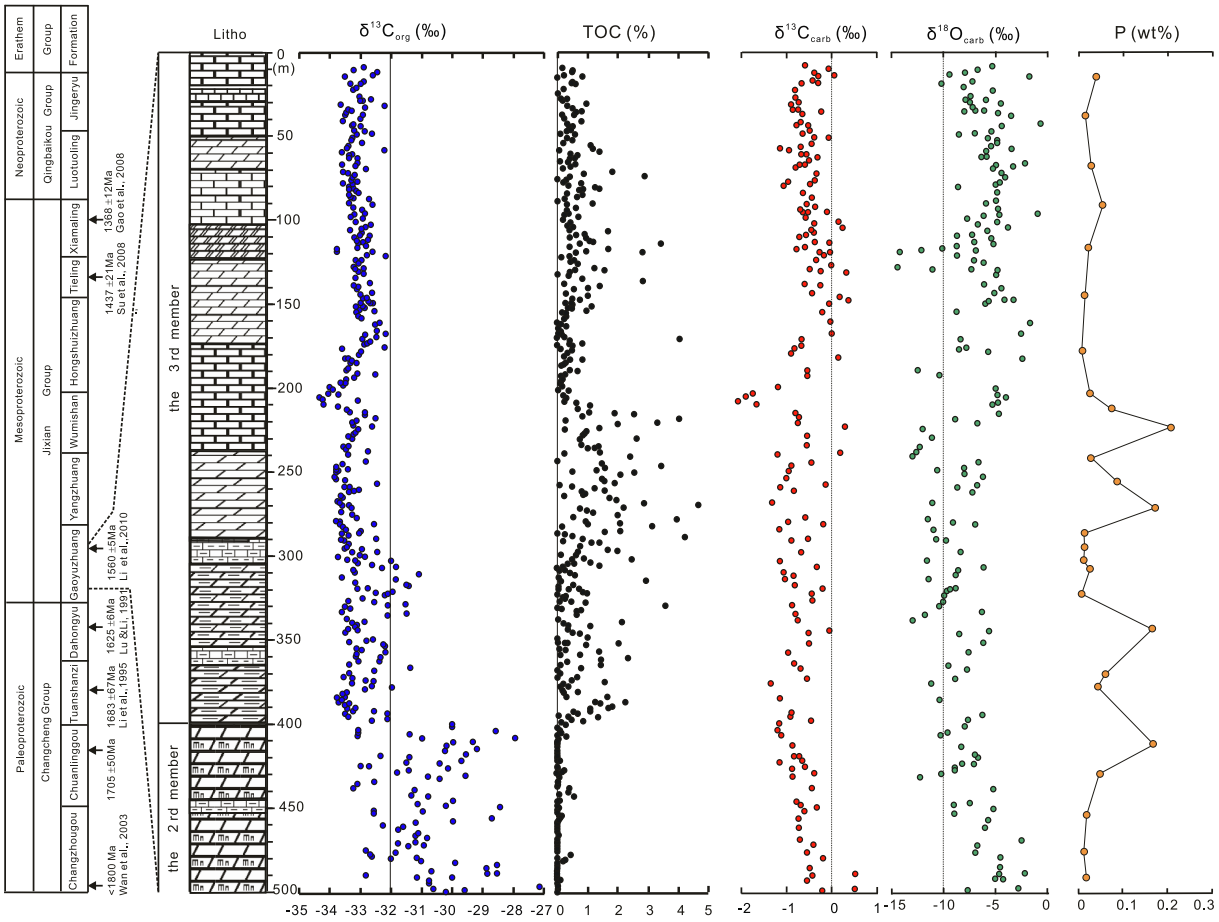

Fig. 3. Records of $\delta^{13}C_{org}$, $\delta^{13}C_{carb}$, $\delta^{18}O_{carb}$, TOC and P contents for the Mesoproterozoic samples of the Gaoyuzhang Formation from North China.

Selden and Edwards, 1989). Second, thermogenic destruction of organic matter associated with hydrocarbon generation can lead to the loss of ^{12}C-enriched carbon and cause the residual organic matter to become enriched in ^{13}C during diagenesis (Hayes et al., 1989; Freeman, 2001); the degree of thermal maturation of the sediment thus influences its bulk organic $\delta^{13}C$ composition. The T_{max} of ~475°C suggests that the thermal maturation of the organic matter in the Gaoyuzhuang Formation has reached a high degree of maturity (Luo et al., 2014). At this level of maturity, thermal alteration of the primary $\delta^{13}C_{org}$ values should be much less than that of metamorphism up to lower greenschist facies, which results in < 3‰ of ^{13}C-enrichment (Simonet et al., 1981; Watanabe et al., 1997). A crossplot of $\delta^{13}C_{org}$ and TOC is widely used to evaluate the influence of organic carbon loss on $\delta^{13}C_{org}$. Our data show little evidence of a linear correlation between $\delta^{13}C_{org}$ and TOC (Fig. 2a), which suggests there is no significant C-isotopic alternation caused by organic carbon loss. Third, organic remineralization can play an important role in the preservation of organic matter in carbonate sediments (Jahnke et al., 1997; Ingalls et al., 2004). $\delta^{13}C_{org}$ in organic-poor carbonates mainly records the isotopic signature of diagenetic alternation or of detrital organic carbon, while that in organic-rich carbonates records the primary isotopic signature of organic carbon (Jiang et al., 2012). Carbonate samples with TOC < 0.1% may not preserve the primary isotopic signal of organic carbon (Fig. 2a).

The oxygen isotope composition of carbonates is readily altered by water–rock reactions during diagenesis (Kaufman and Knoll, 1995). The primary oxygen isotope compositions of carbonates may have been influenced by diagenesis if the $\delta^{18}O$ values are less than −5‰, while they may have been altered by strong diagenesis if the $\delta^{18}O$ values are less than −10 ‰ (Kaufman and Knoll, 1995). C isotopic compositions are often well preserved in Proterozoic carbonates because diagenetic recrystallization of carbonates occurs in a system with a low water/rock ratio for carbon (Kaufman and Knoll, 1995). Additionally, a crossplot of $\delta^{13}C$ and $\delta^{18}O$ (a widely applied indicator to evaluate meteoric alteration), shows little evidence of a linear correlation (Fig. 2b), which indicates no significant C-isotopic alternation by meteoric diagenesis. Organic remineralization in carbonate sediments may also alter the $\delta^{13}C$ of inorganic carbon (Jahnke et al., 1997; Ingalls et al., 2004). A crossplot of $\delta^{13}C_{carb}$ and TOC shows little evidence for a linear correlation, and therefore that there is no significant alternation of the inorganic C-isotopic composition by organic remineralisation (Fig. 2C).

Furthermore, the distinctive trend of both $\delta^{13}C_{carb}$ and $\delta^{13}C_{org}$ and the high reproducibility of the C-isotopic chemostratigraphy of the Gaoyuzhuang Formation (Xiao et al., 1997; Li et al., 2003; Chu et al., 2007; Guo et al., 2013; Luo et al., 2014), as well as the consistency of the carbon isotope stratigraphy with equivalent records from elsewhere (Buick et al., 1995; Kah et al., 1999; Bartley et al., 2007), also suggest that the primary carbon isotopic compositions of the carbonate samples were not subjected to strong alteration. Therefore, we conclude that the original $\delta^{13}C_{carb}$ and $\delta^{13}C_{org}$ signatures were largely preserved in the samples from well JQ3 in the Gaoyuzhuang Formation.

4.2. C-isotope chemostratigraphy

The TOC content from the Gaoyuzhuang Formation varies from 0.01% to 4.65% (Table 1, Fig. 3). Samples from the second member have distinctive TOC contents compared with those from the third member. The samples from the second member, from depths of 500–400 m, have low TOC values of 0.01–0.47%, with an average of 0.07%. The samples from the third member, from depths of 400–8.6 m, have high TOC values, with the range of 0.03–4.65%, with the average of 0.86%.

Table 2
Mesoproterozoic atmospheric CO_2 concentrations calculated according to the $\delta^{13}C_{org}$ and $\delta^{13}C_{carb}$ values from well JQ3 of the Gaoyuzhang Formation.

H(m)	$\delta^{13}C_{carb}$ (‰)	$\delta^{13}C_{org}$ (‰)	ε (20℃)	CO_2 (ppm)	ε (25℃)	CO_2 (ppm)	ε (30℃)	CO_2 (ppm)
8.6	−0.6	−32.9	22.5	1358.2	23.1	2060.9	23.7	3435.4
10.5	−0.1	−33.2	23.4	2142.4	24.0	4012.2	24.6	12461.2
11.8	−0.4	−32.4	22.2	1245.0	22.9	1838.8	23.5	2911.7
13.6	0.0	−32.6	22.8	1567.0	23.4	2504.2	24.1	4665.6
14.3	−0.3	−33.5	23.4	2187.3	24.0	4151.6	24.7	13741.8
17.1	−0.4	−32.9	22.6	1469.0	23.3	2290.5	23.9	4038.2
18.7	−0.3	−33.3	23.2	1972.9	23.9	3516.6	24.5	8958.3
21	−0.7	−33.1	22.6	1425.7	23.2	2199.2	23.8	3790.5
22.3	−0.9	−33.2	22.5	1406.5	23.2	2159.4	23.8	3685.9
26.9	−0.8	−33.0	22.4	1307.9	23.0	1960.8	23.6	3192.8
27.6	−0.8	−32.7	22.1	1177.8	22.7	1712.5	23.3	2636.6
28.3	−0.7	−33.0	22.5	1368.0	23.1	2080.9	23.7	3485.3
28.74	−0.8	−32.9	22.3	1291.2	23.0	1928.0	23.6	3115.5
31	−0.9	−33.6	22.9	1656.7	23.5	2709.5	24.2	5339.0
31.7	−0.8	−32.2	21.6	1009.0	22.2	1411.8	22.8	2039.1
33	−0.7	−32.8	22.3	1282.4	22.9	1910.9	23.6	3075.8
34.1	−0.8	−33.4	22.8	1578.9	23.4	2531.0	24.1	4749.3
34.8	−0.9	−33.3	22.6	1457.1	23.3	2265.3	23.9	3968.7
35.9	−0.3	−33.5	23.4	2215.5	24.1	4241.5	24.7	14660.6
42.5	−0.7	−33.2	22.8	1544.0	23.4	2453.2	24.0	4509.6
43.6	−0.8	−33.3	22.7	1507.1	23.3	2372.3	24.0	4270.4
43.9	−0.5	−33.0	22.7	1493.2	23.3	2342.4	23.9	4184.5
46.3	−0.5	−33.2	22.9	1623.1	23.5	2631.5	24.1	5074.2
46.9	−0.6	−32.8	22.4	1340.8	23.0	2026.0	23.7	3349.6
48.3	−0.7	−32.6	22.1	1194.0	22.7	1742.6	23.4	2700.9
48.7	−0.5	−33.1	22.9	1619.0	23.5	2622.1	24.1	5043.0
51	−0.4	−33.3	23.1	1833.2	23.7	3142.8	24.4	7049.9
51.7	−0.1	−33.3	23.4	2200.7	24.1	4194.4	24.7	14169.0
53.8	−0.5	−33.0	22.7	1479.3	23.3	2312.4	23.9	4099.5
55.6	−0.7	−33.4	22.9	1675.6	23.6	2754.1	24.2	5495.3
57.1	−1.1	−33.4	22.5	1384.8	23.1	2115.0	23.8	3571.6
58.3	−1.0	−32.2	21.4	963.3	22.0	1334.3	22.7	1897.0
59.2	−0.7	−33.6	23.1	1840.3	23.7	3161.3	24.4	7133.5
61.1	−0.6	−33.4	23.0	1740.2	23.6	2909.5	24.3	6073.7
62.5	−0.5	−33.4	23.0	1769.7	23.7	2982.4	24.3	6363.7
63.3	−0.4	−33.1	22.9	1685.1	23.6	2776.5	24.2	5575.8
65.3	−0.5	−33.1	22.8	1551.9	23.4	2470.6	24.0	4562.1
66.7	−0.7	−33.6	23.1	1842.9	23.8	3167.9	24.4	7163.4
67.5	−0.7	−33.2	22.7	1512.2	23.3	2383.5	24.0	4302.9
69	−0.8	−32.8	22.2	1253.1	22.9	1854.3	23.5	2946.6
71.1	−0.4	−33.6	23.4	2221.4	24.1	4260.5	24.7	14865.2
74.1	−0.3	−33.3	23.1	1867.0	23.8	3230.7	24.4	7456.4
76.9	−0.4	−33.1	22.9	1649.5	23.5	2692.7	24.2	5280.9
77.7	−0.9	−33.6	22.9	1608.5	23.5	2598.0	24.1	4963.8
78.8	−0.5	−33.3	23.0	1703.6	23.6	2820.8	24.2	5737.2
80	−1.1	−33.4	22.5	1384.4	23.1	2114.1	23.8	3569.2
83.8	−0.6	−33.1	22.6	1440.2	23.2	2229.7	23.9	3872.0
87.4	−0.5	−32.7	22.5	1361.5	23.1	2067.6	23.7	3452.1
89.7	−0.6	−33.4	23.0	1700.8	23.6	2814.1	24.2	5712.5
92.4	−0.4	−33.2	23.1	1795.6	23.7	3047.0	24.3	6631.9
94	−0.7	−32.9	22.4	1337.6	23.0	2019.7	23.7	3334.2
95.7	−0.1	−32.9	22.9	1671.3	23.6	2743.9	24.2	5459.1
96.5	−0.6	−33.2	22.9	1611.4	23.5	2604.6	24.1	4985.4
97.6	−0.6	−33.3	22.9	1618.8	23.5	2621.6	24.1	5041.3
99.3	−0.6	−32.9	22.5	1398.2	23.2	2142.4	23.8	3641.8
100.8	0.1	−33.2	23.5	2315.3	24.1	4571.9	24.8	18872.4
102.6	−0.4	−32.7	22.4	1348.1	23.1	2040.6	23.7	3385.4
104	0.2	−32.9	23.3	2042.4	23.9	3713.8	24.6	10189.4
105	−0.5	−33.0	22.7	1507.3	23.3	2372.7	24.0	4271.6
105.8	−0.4	−33.3	23.2	1884.8	23.8	3277.7	24.4	7683.4
107.9	−0.4	−33.0	22.7	1512.8	23.3	2384.8	24.0	4306.6
108.7	−0.6	−33.0	22.6	1447.0	23.2	2243.9	23.9	3910.4
109.4	−0.7	−32.7	22.2	1216.0	22.8	1783.8	23.4	2790.0
110.3	−0.7	−33.2	22.7	1505.5	23.3	2368.8	24.0	4260.2
112.3	−0.4	−33.1	22.9	1653.1	23.5	2701.3	24.2	5310.3
113.7	0.0	−33.1	23.2	1965.2	23.9	3495.4	24.5	8835.9
115.1	−0.6	−32.8	22.4	1345.9	23.1	2036.3	23.7	3374.9
116.6	−0.6	−33.1	22.7	1491.3	23.3	2338.2	23.9	4172.3
117.6	−0.8	−33.8	23.2	1959.8	23.9	3480.4	24.5	8750.9
118.4	−0.3	−33.2	23.1	1841.8	23.8	3165.0	24.4	7150.4
118.7	−0.1	−32.6	22.7	1528.3	23.4	2418.5	24.0	4405.7
120.7	−0.2	−32.8	22.8	1560.8	23.4	2490.6	24.0	4623.4
123.5	−0.4	−33.1	23.0	1696.4	23.6	2803.5	24.2	5673.7
125.4	0.0	−33.1	23.2	1964.7	23.9	3494.0	24.5	8827.9

(*continued on next page*)

Table 2 (*continued*)

H(m)	$\delta^{13}C_{carb}$ (‰)	$\delta^{13}C_{org}$ (‰)	ε (20℃)	CO_2 (ppm)	ε (25℃)	CO_2 (ppm)	ε (30℃)	CO_2 (ppm)
127.6	0.0	–33.2	23.4	2133.9	24.0	3985.9	24.6	12237.4
128.9	−0.5	–33.2	22.8	1603.1	23.5	2585.7	24.1	4923.9
129.1	−0.5	–32.9	22.6	1416.3	23.2	2179.8	23.8	3739.1
130.5	−0.3	–33.1	23.0	1732.7	23.6	2891.1	24.3	6002.4
132	0.3	–32.9	23.4	2188.6	24.0	4155.9	24.7	13783.4
137.4	−0.6	–32.7	22.3	1267.2	22.9	1881.5	23.5	3008.4
140.2	−0.2	–33.1	23.1	1786.3	23.7	3023.8	24.3	6534.4
142.7	−0.5	–32.6	22.3	1283.1	22.9	1912.3	23.6	3079.1
146.4	0.2	–32.9	23.3	2041.7	23.9	3711.8	24.6	10175.9
147.6	0.4	–32.7	23.3	2034.4	23.9	3690.9	24.6	10036.8
148.5	0.3	–32.7	23.3	1977.4	23.9	3529.1	24.5	9031.0
149	−0.1	–32.6	22.7	1497.6	23.3	2351.9	23.9	4211.5
154.3	−0.2	–32.5	22.5	1411.4	23.2	2169.6	23.8	3712.4
161.1	0.0	–32.4	22.5	1377.5	23.1	2100.1	23.7	3533.7
167.4	0.0	–32.2	22.3	1292.9	23.0	1931.4	23.6	3123.7
171	−0.7	–32.9	22.4	1336.4	23.0	2017.2	23.7	3328.1
175.6	−0.7	–32.2	21.7	1033.2	22.3	1453.5	22.9	2117.5
176.5	−0.9	–33.6	23.0	1697.2	23.6	2805.4	24.2	5680.8
178.2	−0.9	–33.0	22.3	1282.4	22.9	1911.0	23.6	3076.1
182	−0.1	–33.1	23.2	1907.7	23.8	3338.6	24.4	7988.9
188.6	−0.6	–33.4	23.1	1806.3	23.7	3074.1	24.3	6747.8
199.7	−1.2	−34.0	23.0	1754.9	23.7	2945.6	24.3	6215.8
202.7	−1.8	−34.0	22.5	1379.2	23.1	2103.5	23.8	3542.3
205.2	−1.9	−34.3	22.7	1478.6	23.3	2311.0	23.9	4095.7
207.3	−2.1	–33.1	21.2	909.5	21.8	1245.0	22.5	1738.7
209.5	−1.7	−34.2	22.8	1557.8	23.4	2483.7	24.0	4602.3
215.3	−0.8	–32.8	22.2	1244.6	22.8	1838.0	23.5	2909.9
218	−0.7	–32.5	22.0	1152.2	22.6	1665.5	23.3	2538.0
220.2	−0.8	–33.3	22.7	1503.8	23.3	2365.3	24.0	4250.1
223	0.3	–32.6	23.1	1824.0	23.7	3119.2	24.4	6944.5
228.7	−0.5	–33.4	23.0	1764.4	23.7	2969.2	24.3	6310.3
234.5	−0.6	–33.5	23.2	1903.2	23.8	3326.7	24.4	7928.0
237.6	0.2	–32.7	23.1	1837.6	23.7	3154.3	24.4	7101.7
239.5	−1.2	–33.4	22.4	1321.3	23.0	1987.2	23.6	3255.7
243.8	−0.5	–32.8	22.5	1390.4	23.1	2126.4	23.8	3600.7
247.3	−0.9	–33.8	23.1	1815.4	23.7	3097.4	24.4	6848.6
248.3	−1.0	–33.4	22.6	1454.1	23.3	2258.9	23.9	3951.2
252.2	−1.0	–33.9	23.1	1786.1	23.7	3023.1	24.3	6531.6
256.7	−0.1	–32.4	22.5	1365.9	23.1	2076.5	23.7	3474.3
258.4	−1.2	–33.5	22.5	1395.0	23.1	2135.9	23.8	3625.1
260.7	−0.8	–33.1	22.4	1343.7	23.1	2031.9	23.7	3363.9
267.6	−1.3	–33.7	22.6	1449.6	23.2	2249.3	23.9	3925.1
277.4	−0.6	–33.1	22.8	1538.6	23.4	2441.2	24.0	4473.3
278.8	−1.0	–33.8	23.0	1741.9	23.6	2913.7	24.3	6090.1
281	−0.2	–32.6	22.5	1403.9	23.2	2154.1	23.8	3672.1
283	−1.2	–33.6	22.6	1443.0	23.2	2235.4	23.9	3887.5
290.2	−0.9	–33.6	22.9	1675.3	23.6	2753.4	24.2	5492.9
308.1	−1.1	–33.2	22.3	1299.5	23.0	1944.3	23.6	3153.8
312.8	−1.0	–33.6	22.8	1576.0	23.4	2524.4	24.1	4728.5
319.3	−0.2	–33.1	23.1	1804.1	23.7	3068.6	24.3	6723.8
326.5	−0.4	–33.4	23.2	1916.6	23.8	3362.6	24.5	8112.4
332.7	−0.8	–33.6	23.0	1699.7	23.6	2811.5	24.2	5703.1
337.5	−0.8	–33.5	22.9	1652.6	23.5	2699.9	24.2	5305.6
343.9	−0.1	–33.1	23.2	1941.8	23.8	3430.9	24.5	8476.0
345.6	−0.5	–33.5	23.2	1910.9	23.8	3347.2	24.4	8032.9
351	−0.5	–33.4	23.0	1770.0	23.7	2982.9	24.3	6366.1
364.3	−0.9	–33.4	22.7	1513.1	23.3	2385.4	24.0	4308.4
372	−0.6	–33.5	23.2	1891.7	23.8	3295.8	24.4	7773.0
384.4	−1.1	–33.8	22.9	1618.8	23.5	2621.6	24.1	5041.2
393.7	−1.0	–32.1	21.3	935.8	21.9	1288.3	22.6	1814.7
393.76	−0.9	–33.5	22.9	1608.8	23.5	2598.7	24.1	4966.1
419.1	−0.7	–32.4	21.8	1071.4	22.4	1520.4	23.0	2246.1
425.4	−0.6	–33.0	22.6	1424.2	23.2	2196.1	23.8	3782.4
438	−0.4	–33.2	23.0	1719.3	23.6	2858.5	24.2	5878.3
451.7	−0.6	–32.6	22.1	1194.3	22.7	1743.1	23.4	2701.9
475.2	−0.6	–32.8	22.4	1344.2	23.1	2032.8	23.7	3366.1
490.15	−0.5	–32.8	22.5	1369.5	23.1	2083.8	23.7	3492.6

Consistent with the TOC values, the $\delta^{13}C_{org}$ values from the second member of the Gaoyuzhuang Formation are different from those of the third member (Fig, 3). The $\delta^{13}C_{org}$ values from the depths of 500–400 m vary within the large range of −27.1‰ to –33.2‰, with the average of −30.9‰; while the samples from the third member, from depths < 400 m, have lower $\delta^{13}C_{org}$ values, within the range of −34.3‰ to −31.1‰, and with an average of –33.1‰. There are two negative excursions of $\delta^{13}C_{org,}$ at the depths of ~400 m and ~200 m.

The $\delta^{13}C_{carb}$ values of the Gaoyuzhuang Formation vary within the range of −2.1‰ to 0.94‰, and show two negative excursions, at the depths of ~400 m and ~200 m. Within the depth interval of 400–390 m, the $\delta^{13}C_{carb}$ values decrease from 0.5‰ to −2.0‰ (Fig. 3), with a 2.5‰

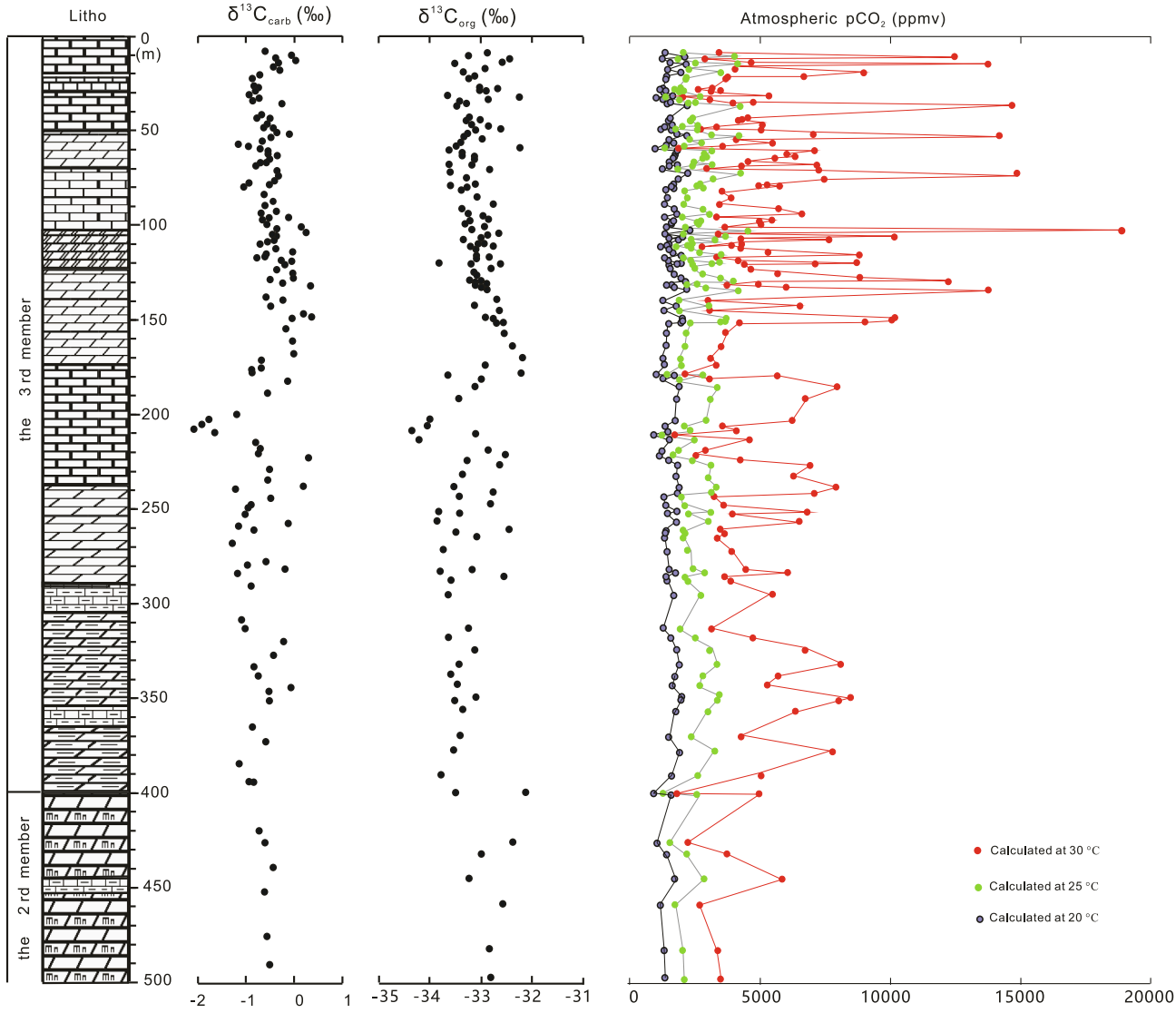

Fig. 4. Mesoproterozoic atmospheric CO_2 concentrations estimated from the values of $\delta^{13}C_{org}$ and $\delta^{13}C_{carb}$ of the samples from well JQ3 of the Gaoyuzhang Formation in North China.

negative excursion. Within the interval of 223–199 m, the $\delta^{13}C_{carb}$ values decrease from 0.3‰ to −2.1‰ (Fig. 3), with a 2.4‰ negative excursion. Overall, the $\delta^{13}C_{carb}$ and $\delta^{13}C_{org}$ values co-vary, which suggests that the carbon isotope data mainly reflect changes in primary productivity and the burial of organic carbon during the Early Mesoproterozoic.

4.3. Estimation of the atmospheric CO_2 concentration

Well-preserved primary isotopic profiles record changes not only in the burial of organic carbon, but also in atmospheric CO_2 concentrations (Kump and Arthur, 1999). The isotopic difference between the burial organic carbon and carbonate (Δ_B) can be used as a rough proxy for atmospheric pCO_2 in the geological past (Dean et al., 1986; Freeman and Hayes, 1992). Accurate atmospheric CO_2 concentrations need to be calculated using specific methods. The paired $\delta^{13}C_{org}$ and $\delta^{13}C_{carb}$ values from well JQ3 potentially enable us to constrain the atmospheric pCO_2 of the Mesoproterozoic (Kump and Arthur, 1999).

Many attempts have been made to calibrate the photosynthetic isotopic effect (Ɛp) for marine algae against CO_2 concentration (Freeman and Hayes, 1992; Laws et al., 1995; Bidigare et al., 1997; Popp et al., 1998; Pagani et al., 1999). Laws et al. (1995) and Bidigare et al. (1997), using the results of analyses of marine microalgae grown in chemostat cultures, established systematic quantitative relationships between cell growth rate, [CO_2(aq)] and carbon isotopic fractionation. Popp et al. (1998) suggested that Ɛp is not only related with Ce, growth rate, but also with phytoplankton cell geometry; Pagani et al. (1999) fitted the data using a geometric mean assumption and developed an equation for Ɛp and Ce, assuming a maximum enzymatic isotope effect of 25 ‰. Taking advantage of this method, Pagani et al. (1999) reconstructed Late Oligocene to Late Miocene pCO_2 from Ɛp values based on carbon isotopic analyses of organic matters and planktonic foraminifera from sediments from ocean drilling sites. The method developed by Pagani et al. (1999) is suitable for studying ancient rock samples, and therefore we used it to estimate the Mesoproterozoic atmospheric pCO_2, as follows:

$$(25\text{-}\ \varepsilon p)Ce = 116.96[PO_4^{3-}] + 81.42$$

$$\varepsilon p = [(\delta_{CO2(aq)} + 1000)/(\delta_{org} + 1000)\text{-}1] \times 1000$$

$$\varepsilon_{calcite\text{-}CO2(g)} = [(\delta_{calcite} + 1000)/(\delta co_{2(g)} + 1000)\text{-}1] \times 1000 = 11.98\text{–}0.12*T\ (℃)$$

$$\varepsilon_{CO2(aq)\text{–}CO2(g)} = [(\delta_{CO2(aq)} + 1000)/(\delta_{co2(g)} + 1000)\text{-}1] \times 1000 = -373/T(K) + 0.19$$

Here, the phosphate concentration [PO_4^{3-}] is regarded as the nutrient input. Owing to the low atmospheric oxygen level, the Mesoproterozoic seawater phosphate concentration could have been much lower than that in the modern ocean (Anbar and Knoll, 2002; Reinhard et al., 2016). It was estimated that phosphorus concentrations in Mesoproterozoic sediments vary within the range of 0.01–0.68% (Reinhard et al., 2016). We measured the phosphorus concentrations in 27 samples from the Gaoyuzhuang Formation and found that they vary within the range of 0.01–0.46%. We selected a typical oligotrophic surface-ocean value, [PO_4^{3-}] = 0.25 μmol/kg, to calculate the dissolved CO_2 concentration (Ce) (Kump and Arthur, 1999).

According to Henry's Law, we can calculate atmospheric pCO_2 using the equation $pCO_2 = Ce/K_H$, where K_H is the CO_2 solubility coefficient that is a function of the salinity and temperature of seawater. For a seawater salinity of 35‰ (a typical modern seawater salinity value), K_H = 0.032 mol/kg·atm at 20°C, K_H = 0.028 mol/kg•atm at 25°C, and K_H = 0.025 mol/kg•atm at 30°C (Weiss, 1974).

If the surface seawater temperature were 20°C during the Mesoproterozoic, the atmospheric CO_2 concentration was estimated to be within the range of 910–2315 ppm, with an average of 1582 ppm (Table 2; Fig. 4). At 25°C, atmospheric CO_2 concentration was estimated to be within the range of 1245– 4572 ppm, with an average of 2588 ppm (Table 2; Fig. 4). At 30°C, the atmospheric CO_2 was estimated to be within the range of 1738–18,872 ppm, with an average of 5437 ppm (Table 2; Fig. 4). It can be seen that pCO_2 calculated for 30°C varies within a large range, while that calculated for 20°C and 25°C varies within relatively small range.

4.4. Uncertainties in the pCO_2 calculations

Although diagenetic influences on carbon isotope compositions in organic matter and carbonates could cause deviation from the primary photosynthetic isotope effect (Ɛp), sufficient $\delta^{13}C_{org}$ and $\delta^{13}C_{carb}$ data for a given interval can still provide a record of changes in atmospheric pCO_2 (Kump and Arthur, 1999). Seawater [PO_4^{3-}] is another factor that could influence the calculated atmospheric pCO_2 values. If the selected [PO_4^{3-}] is less than the true concentration in the Mesoproterozoic ocean, the calculated atmospheric pCO_2 will also be lower than the primary pCO_2, and vice versa. Mesoproterozoic seawater phosphorus concentrations cannot be measured directly, and we can only infer them from the phosphorus concentrations in Mesoproterozoic sediments. Based on the measurements of sedimentary phosphorus concentrations combined with the data from the literature, we suggest that the selected seawater [PO_4^{3-}] = 0.25 μmol/kg (a typical oligotrophic modern surface ocean value) is a reasonable estimate of the Mesoproterozoic seawater phosphorus concentration.

Lastly, the value of Ɛp and the Henry's Law constant are related to the seawater temperature. We chose temperatures of 20°C, 25°C, and 30°C as the sea surface temperature. 25°C is a reasonable average low-latitude temperature (Kump and Arthur, 1999; Kaufman and Xiao, 2003). The North China craton was suggested to be at a low latitude during the Mesoproterozoic (Zhao et al., 2004), and therefore 20–30°C may be reasonable a range for Mesoproterozoic sea surface temperatures. It is possible that the modern calibration of atmospheric pCO_2 was different from that in the Mesoproterozoic. Differences can potentially be attributed to factors such as differences in planktonic species and the oceanic environment.

4.5. Implications of the results for the Mesoproterozoic environment

According to our calculations, the Mesoproterozoic atmospheric pCO_2 levels are much higher than that of the modern atmosphere. If the Mesoproterozoic solar luminosity was close to that for the modern Earth, the high atmospheric pCO_2 levels suggest a greenhouse environment during the Mesoproterozoic. However, at 25°C (a reasonable average low-latitude temperature), the atmospheric pCO_2 levels calculated in this study are up to 3–10 times those of the PAL. The increase in atmospheric pCO_2 concentrations from ~280 ppmv to 400 ppmv has played a major role in the enhanced greenhouse effect since the Industrial Revolution. This indicates that solar luminosity during the Mesoproterozoic was much lower than that for the modern Earth, which is consistent with an atmospheric and climate model of the early Earth (Kasting, 1993). High atmospheric pCO_2 levels could have played an important role in compensating for lower solar luminosity and maintaining a normal temperature on the Mesoproterozoic Earth's surface.

5. Conclusions

High-resolution $\delta^{13}C_{org}$ and $\delta^{13}C_{carb}$ measurements of well-preserved samples from well JQ3 have recorded primary isotopic signals that are linked to the carbon biogeochemical cycle and can help constrain the atmospheric pCO_2 during the Mesoproterozoic. The ~1.6 Ga paired carbonate and organic carbon isotope records indicate high atmospheric CO_2 concentrations during the Mesoproterozoic, suggesting a greenhouse environment or lower solar luminosity.

Declaration of Competing Interest

The authors declare that they have no known competing financial interests or personal relationships that could have appeared to influence the work reported in this paper.

Acknowledgements

This work was supported by the National Natural Science Foundation of China (41272041, 41721002, 41890842, 42103073, 42103074), National Postdoctoral Program for Innovative Talents of China (BX2021278). Measurements of C-isotopes were carried out at the State Key Laboratory of Petroleum Resource and Prospecting, China University of Petroleum, Beijing. We thank two anonymous reviewers for their thoughtful comments that have greatly improved this paper.

References

Anbar, A.D., Knoll, A.H., 2002. Proterozoic ocean chemistry and evolution: a bioinorganic bridge? Science 297, 1137–1143.
Awramik, S.M., Sprinkle, J., 1999. Proterozoic stromatolites: the first marine evolutionary biota. Hist. Biol. 13, 241–253.
Bartley, J.K., Kah, L.C., McWilliams, J.L., Stagner, A.F., 2007. Carbon isotope chemostratigraphy of the Middle Riphean type section (Avzyan Formation, Southern Urals, Russia): signal recovery in a fold-and-thrust belt. Chem. Geol. 237, 211–232.
Bidigare, R.R., Fluegge, A., Freeman, K.H., Hanson, K.L., Hayes, J.M., Hollander, D., Jasper, J.P., King, L.L., Laws, E.A., Milder, J., Millero, F.J., Pancost, R., Popp, B.N., Steinberg, P.A., Wakeham, S.G., 1997. Consistent fractionation of ^{13}C in nature and in the laboratory: Growth-rate effects in some haptophyte algae. Global Biogeochem. Cycles 11, 279–292.
Buick, R., Des Marais, D.J., Knoll, A.H., 1995. Stable isotopic compositions of carbonates from the Mesoproterozoic Bangemall Group, northwestern Australia. Chem. Geol. 123, 153–171.
Butterfield, N.J., 2009. Oxygen, animals and oceanic ventilation: an alternative view. Geobiology 7, 1–7.
Chen, J., Zhang, H., Zhu, S., Zhao, Z., Wang, Z., 1980. Research on Sinian Suberathem of Jixian Tianjin (in Chinese). In: Research on Precambrian Geology: Sinian Suberathem in China. Tianjin Sci. & Tech. Press, Tianjin, pp. 56–114.
Chu, X., Zhang, T., Zhang, Q., Lyons, T., 2007. Sulfur and carbon isotope records from 1700 to 800Ma carbonates of the Jixian section, northern China: implications for secular isotope variations in Proterozoic seawater and relationships to global superconitinental events. Geochim. Cosmochim. Acta 71, 4668–4692.
Dean, E.D., Arthur, M.A., Claypool, G.E., 1986. Depletion of ^{13}C in Cretaceous marine organic matter: source, diagenetic, or environmental signal? Mar. Geol. 7, 119–157.
Douzery, E.J.P., Snell, E.A., Bapteste, E., Delsuc, F., Philippe, H., 2004. The timing of eukaryotic evolution: does a relaxed molecular clock reconcile proteins and fossils? Proc. Natl. Acad. Sci. U. S. A. 101, 15386–15391.
Droser, M.L., Tarhan, L.G., Gehling, J.G., 2017. The Rise of Animals in a Changing Environment: Global Ecological Innovation in the Late Ediacaran. Annu. Rev. Earth Planet. Sci. 45, 593–617.
Farquhar, J., Bao, H., Thiemens, M., 2000. Atmospheric influence of earth's earliest sulfur cycle. Science 289, 756–758.
Freeman, K.H., 2001. Isotopic biogeochemistry of marine organic carbon. Rev. Mineral. Geochem. 43, 579–605.

Freeman, K.H., Hayes, J.M., 1992. Fractionation of carbon isotopes by phytoplankton and estimates of ancient CO_2 levels. Global Biogeochem. Cycles 6, 185–198.
Grotzinger, J.P., 1990. Geochemical model for Proterozoic stromatolite decline. Am. J. Sci. 290-A, 80–103.
Guo, H., Du, Y., Kah, L., Huang, J., Hu, C., Huang, H., Yu, W., 2013. Isotopic composition of organic and inorganic carbon from the Mesoproterozoic Jixian Group, North China: implications for biological and oceanic evolution. Precambrian Res. 224, 169–183.
Hayes, J.M., Popp, B.N., Takigiku, R., Johnson, M.W., 1989. An isotopic study of biogeochemical relationships between carbonates and organic carbon on the Greenhorn Formation. Geochim. Cosmochim. Acta 68, 4363–4379.
Hoffman, P.F., Kaufman, A.J., Halverson, G.P., Schrag, D.P., 1998. A Neoproterozoic snowball Earth. Science 281, 1342–1346.
Hoffman, P.F., Abbot, D.S., Ashkenazy, Y., Benn, D.I., Brocks, J.J., Cohen, P.A., Cox, G. M., Creveling, J.R., Donnadieu, Y., Erwin, D.H., Fairchild, I.J., Ferreira, D., Goodman, J.C., Halverson, G.P., Jansen, M.F., Le Hir, G., Love, G.D., Macdonald, F. A., Maloof, A.C., Partin, C.A., Ramstein, G., Rose, B.E.J., Rose, C.V., Sadler, P.M., Tziperman, E., Voigt, A., Warren, S.G., 2017. Snowball Earth climate dynamics and Cryogenian geology-geobiology. Sci. Adv. 3, e1600983.
Ingalls, A.E., Aller, R.C., Lee, C., Wakeham, S.G., 2004. Organic matter diagenesis in shallow water carbonate sediments. Geochim. Cosmochim. Acta 68, 4363–4379.
Jahnke, R.A., Craven, D.B., McCorkle, D.C., Reimers, C.E., 1997. $CaCO_3$ dissolution in California continental margin sediments: The influence of organic matter remineralization. Geochim. Cosmochim. Acta 61, 3587–3604.
Jiang, G., Wang, X., Shi, X., Xiao, S., Zhang, S., Dong, J., 2012. The origin of decoupled carbonate and organic carbon isotope signatures in the early Cambrian (ca. 542–520Ma) Yangtze platform. Earth Planet. Sci. Lett. 317, 96–110.
Kah, L.C., Bartley, J.K., 2011. Protracted oxygenation of the Proterozoic biosphere. Int. Geol. Rev. 53, 1424–1442.
Kah, L.C., Sherman, A.G., Narbonne, G.M., Knoll, A.H., Kaufman, A.J., 1999. $\delta^{13}C$ stratigraphy of the Proterozoic Bylot Supergroup, Baffin Island, Canada: implications for regional lithostratigraphic correlations. Can. J. Earth Sci. 36, 313–332.
Kasting, J.F., 1993. Earth's early atmosphere. Science 259, 920–926.
Kasting, J.F., Ono, S., 2006. Palaeoclimates: the first two billion years. Philos. Trans. R. Soc. B 361, 917–929.
Kaufman, A.J., Knoll, A.H., 1995. Neoproterozoic variations in the C-isotopic composition of seawater: stratigraphic and biogeochemical implications. Precambrian Res. 73, 27–49.
Kaufman, A.J., Xiao, S., 2003. High CO_2 levels in the Proterozoic atmosphere estimated from analyses of individual microfossils. Nature 425, 279–282.
Kump, L.R., Arthur, M.A., 1999. Interpreting carbon-isotope excursions: carbonates and organic matter. Chem. Geol. 161, 181–198.
Laws, E.A., Popp, B.N., Bidigare, R.R., Kennicut, M.C., Macko, S.A., 1995. Dependence of phytoplankton carbon isotopic composition on growth rate and $[CO_2aq]$: theoretical considerations and experimental results. Geochim. Cosmochim. Acta 59, 1131–1138.
Li, R., Chen, J., Zang, S., Chen, Z., 2003. Secular variations in carbon isotopic compositions of carbonates from Proterozoic successions in the Ming Tombs Section of the North China Platform. J. Asian Earth Sci. 22, 329–341.
Li, H., Zhu, S., Xiang, Z., Su, W., Lu, S., Zhou, H., Geng, J., Li, S., Yang, F., 2010. Zircon U-Pb dating on tuff bed from Gaoyuzhuang Formation in Yanqing, Beijing: further constraints on the new subdivision of the Mesoproterozoic stratigraphy in the northern North China Craton. Acta Petrol. Sin. 26, 2131–2140 (in Chinese with English abstract).
Lu, S., Yang, C., Zhu, S., Mei, H., 1996. Precambrian continental crust profile from eastern Hebei to Jixian Tianjin. In: Hou, H. (Ed.), Proceedings of the 30th International Geological Congress. Geological Publishing House, Beijing, pp. T105.1–T105.42.
Lu, S., Li, H., 1991. A precise U-Pb single zircon age determination for the volcanics of the Dahongyu Formation Changcheng System in Jixian. Bull. Chin. Acad. Geol. Sci. 22, 137–146 (in Chinese with English abstract).
Lu, S., Zhao, G., Wang, H., Hao, G., 2008. Precambrian metamorphic basement and sedimentary cover of the North China Craton: a review. Precambrian Res. 160, 77–93.
Luo, G., Junium, C., Kump, L., Huang, J., Li, C., Feng, Q., Shi, X., Bai, X., Xie, S., 2014. Shallow stratification prevailed for ~1700 to ~1300Ma ocean: Evidence from organic carbon isotopes in the North China Craton. Earth Planet. Sci. Lett. 400, 219–232.
Pagani, M., Arthur, M., Freeman, K., 1999. Miocene evolution of atmospheric carbon dioxide. Paleoceanography 14, 273–292.
Popp, B.N., Takigiku, R., Hayes, J.M., Louda, J.W., Baker, E.W., 1989. The post-Paleozoic chronology and mechanism of ^{13}C depletion in primary marine organic matter. Am. J. Sci. 289, 436–454.
Popp, B.N., Laws, E.A., Bidigare, R.R., Dore, J.E., Hanson, K.L., Wakeham, S.G., 1998. Effect of phytoplankton cell geometry on carbon isotopic fractionation. Geochim. Cosmochim. Acta 62, 69–77.
Rau, G.H., Takahashi, T., Des Marais, D.J., 1989. Latitudinal variations in plankton $\delta^{13}C$: implications for CO_2 and productivity in past oceans. Nature 341, 516–518.
Reinhard, C.T., Planavsky, N.J., Gill, B.C., Ozaki, K., Robbins, L.J., Lyons, T.W., Fischer, W.W., Wang, C., Cole, D.B., Konhauser, K.O., 2017. Evolution of the global phosphorus cycle. Nature 541, 386–389.
Retallack, G.J., Chen, Z., Huang, Y., Fang, Y., 2021. Oxidizing atmosphere and life on land during the late Paleoproterozoic outset of the "boring billion". Precambrian Res. 364, 106361.
Riding, R., 2000. Microbial carbonates: the geological record of calcified bacterial-algal mats and biofilms. Sedimentology 47 (Suppl. 1), 179–214.
Rogers, J.J.W., Santosh, M., 2002. Configuration of Columbia a Mesoproterozoic supercontinent. Gondwana Res. 5, 5–22.
Schopf, J.W., Klein, C. (Eds.), 1992. The Proterozoic biosphere. Cambridge University Press, New York, pp. 1–1374.
Selden, P.A., Edwards, D., 1989. Colonisation of the land. In: Allen, K., Briggs, D. (Eds.), Evolution and the Fossil Record. Belhaven, London, pp. 122–152.
Sheldon, N.D., 2006. Precambrian paleosols and atmospheric CO_2 levels. Precambrian Res. 147, 148–155.
Sheldon, N.D., 2013. Causes and consequences of low atmospheric pCO_2 in the Late Mesoproterozoic. Chem. Geol. 362, 224–231.
Sheldon, N.D., Mitchell, R.L., Dzombak, R.M., 2021. Reconstructing Precambrian pCO_2 and pO_2 using paleosols. In: Elements in Geochemical Tracers in Earth System Science. Cambridge University Press, pp. 1–28.
Simonet, B.R.T., Brenner, S., Peters, K.E., Kaplan, I.R., 1981. Thermal alteration of Cretaceous black shale by diabase intrusions in the Eastern Atlantic: II. Effects on bitumen and kerogen. Geochim. Cosmochim. Acta 45, 1581–1602.
Watanabe, Y., Naraoka, H., Wronkiewicz, D.J., Condie, K.C., Ohmoto, H., 1997. Carbon, nitrogen, and sulfur geochemistry of Archean and Proterozoic shales from the Kaapvaal Craton. South Africa. Geochim. Cosmochim. Acta 61, 3441–3459.
Weiss, R.F., 1974. Carbon dioxide in water seawater: the solubility of a non-ideal gas. Mar. Chem. 2, 203–215.
Xiao, S., Knoll, A.H., Kaufman, A.J., Yin, L., Zhang, Y., 1997. Neoproterozoic fossils in Mesoproterozoic rocks? Chemostratigraphic resolution of a biostratigraphic conundrum from the North China Platform. Precambrian Res. 84, 197–220.
Xiao, S., Laflamme, M., 2009. On the eve of animal radiation: phylogeny, ecology and evolution of the Ediacara biota. Trends Ecol. Evol. 24, 31–40.
Zhao, C., Li, R., Zhou, J., 1997. Sedimentology and petroleum geology of the Meso-and Neo-Proterozoic in North China. Geological Publishing House, Beijing (in Chinese with English abstract).
Zhao, G., Sun, M., Wilde, S.A., Li, S., 2004. A Paleo-Mesoproterozoic supercontinent: assembly, growth and breakup. Earth-Sci. Rev. 67, 91–123.
Zhu, S., Xing, Y., Zhang, P., 1996. Biostratigraphic sequence of the middle-upper Proterozoic on north China Platform. Geological Publishing House, Beijing (in Chinese with English abstract).
Zhu, S., Huang, X., Sun, S., 2005. New progress in the research of the Meso-proterozoic Changcheng System (1800–1400Ma) in the Yanshan range, North China. J. Stratigr. 29, 437–449 (in Chinese with English abstract).